Journal of Catalysis **208,** 21–29 (2002)
doi:10.1006/jcat.2002.3547, available online at http://www.idealibrary.com on IDEAL®

Effects of Methane and Ethane on the Heterogeneous Production of Water from Hydrogen and Oxygen over Platinum in Stagnation Flow

Anthony H. McDaniel,[1] Andrew E. Lutz, Mark D. Allendorf, and Steven F. Rice

Combustion Research Facility, Sandia National Laboratories, MS 9052, P.O. Box 969, Livermore, California 94550

Received July 3, 2001; revised January 30, 2002; accepted January 30, 2002

The effects of CH_4 and C_2H_6 on the catalytic production of water from hydrogen-rich mixtures are investigated in a stagnation flow reactor using a combination of experimental and numerical methods. The analytical treatment assesses the accuracy of a detailed elementary reaction mechanism recently proposed for partial oxidation of ethane in short-contact-time reactors. Both CH_4 and C_2H_6 inhibit the heterogeneous water-forming chemistry, as evidenced by a strong correlation between the net water production, light-off temperature, and mole fraction of hydrocarbon in the reactor. The effects of C_2H_6 on Pt are more pronounced than those of CH_4, due to its propensity for forming carbonaceous overlayers on the catalyst surface. A general kinetic mechanism used successfully to describe partial oxidation of C_2H_6 over Pt-impregnated monoliths could not reproduce the experimental observations. Discrepancies between model chemistry and experiment reveal possible avenues for the improvement of the mechanism. © 2002 Elsevier Science (USA)

Key Words: **platinum; partial oxidation; kinetic model; methane; ethane; hydrogen; inhibition; stagnation flow.**

1. INTRODUCTION

The oxidation of hydrogen and hydrocarbons over noble metal catalysts is an area of research that is rich with complexity. In recent years, several technologically important applications have emerged that exploit the product selectivity and ignition-control characteristics of catalytic combustion. Most notable are new autothermal processes for generating synthesis gas from methane (1, 2) or dehydrogenating ethane to ethylene (3) via partial oxidation of rich hydrocarbon feeds in short-contact-time reactors (SCTR). It is common for catalytic metals such as platinum, palladium, and rhodium to be used near stoichiometry for exhaust-gas aftertreatment (4, 5) or as initiators of fuel-lean combustion in heat and power generation (6). Operating these materials under fuel-rich, reducing environments can have pronounced effects on reactivity, because the extent of surface oxidation ultimately determines the rate of C–H bond activation (7). Understanding this complex behavior is important to the successful commercialization of these advanced applications.

To date, research into the catalytic oxidation of H_2 over platinum has matured to the point where reliable kinetic mechanisms that span a wide range of operating conditions are available (8–12). However, an in-depth understanding of the complex surface chemistry prevalent in fuel-rich partial oxidation of hydrocarbons is lacking, primarily because this field of research is relatively new. While a small number of detailed kinetic mechanisms for both C_1 and C_2 systems are available (1, 13–19), due in part to the efforts of Wolf, Deustchmann, Schmidt, and Warnatz, they are largely interrelated, making a general consensus on important reaction pathways and kinetic parameters difficult to formulate. What is needed at this point is to validate the predictive capabilities of these multistepped reaction schemes, under experimental conditions sufficiently different from those used to derive them, in order to expose areas for improvement and thereby enhance their reliability and usefulness.

This work investigates the effects of CH_4 and C_2H_6 on the heterogeneous production of water over Pt under hydrogen-rich conditions. In so doing, we offer an argument that the presence of small quantities of hydrocarbon inhibits the hydrogen oxidation chemistry. At the outset, this idea may seem contrary to the conventional wisdom that water inhibits hydrocarbon oxidation, which has been observed for CH_4 on Pd (7, 20, 21) and C_3H_6 on Pt (22). However, the definition of inhibitor and/or promoter is predicated on the condition of the catalyst as well as on the intent of the experiment. We contend that the hydrocarbon inhibition reported here under hydrogen-rich conditions is the result of hydrocarbon being a minority reactant in an experiment designed to look at the autothermal behavior of hydrogen oxidation.

The $H_2 : O_2 : C_xH_{2x+2}$/Pt system ($x = 1, 2$) is scrutinized under hydrogen-rich conditions by a coupled approach involving both experimental and numerical methods. In the experiment, a low-pressure stagnation flow reactor is used as an ideal system for probing the heterogeneous chemistry without interference from gas-phase reactions. In addition, the experimental setup is amenable to lower dimensional modeling, which facilitates the incorporation of detailed,

[1] To whom correspondence should be addressed. Fax: 925-294-2276. E-mail: amcdani@sandia.gov.

0021-9517/02 $35.00

many-step reaction mechanisms. Experimental measurements are compared directly to numerical predictions, and discrepancies between the two are discussed within the context of the investigation.

2. EXPERIMENTAL

Apparatus and Measurements

The experimental apparatus is depicted in Fig. 1 and consists of a stainless-steel vacuum chamber interfaced to a quadrupole mass spectrometer (Inficon Transpector 300H). The chamber is equipped with a gas-handling manifold, a cylindrical substrate pedestal, electrical feedthroughs for power and thermocouple signals, windows for optical access, and roughing components for exhaust control. Feed gas enters from the bottom of the reactor and impinges onto a downward-facing catalytic substrate, thereby creating a stagnation plane. Buoyancy effects induced by thermal gradients that exist between the heated substrate and the cold walls are minimized by the upward direction of the flow.

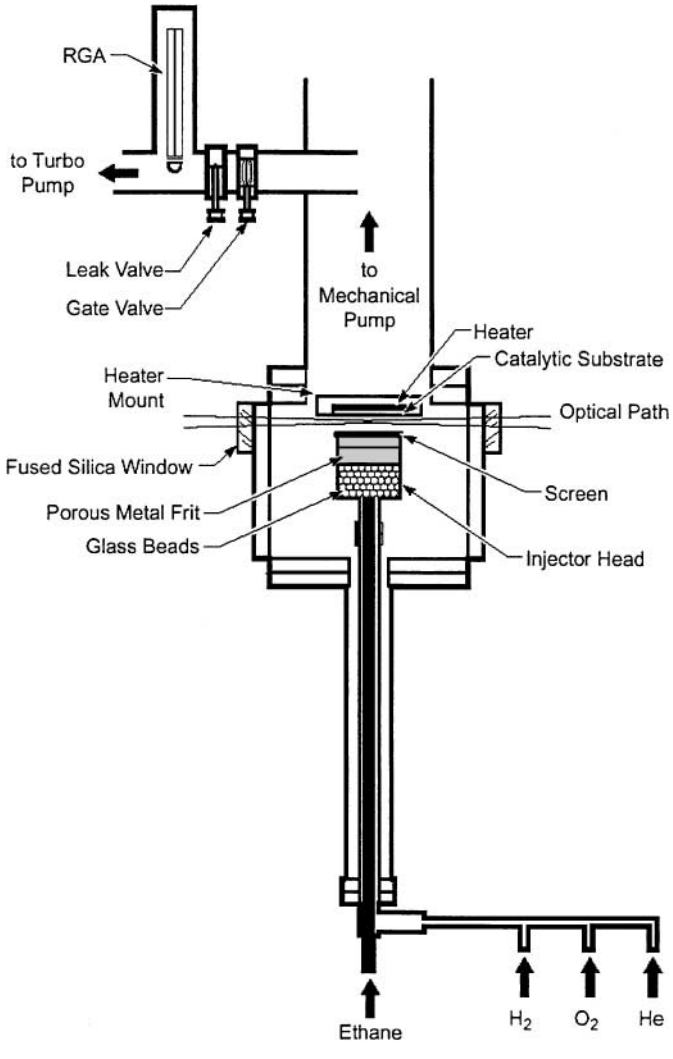

FIG. 1. Schematic of the experimental apparatus showing the stagnation flow reactor, inlet manifold, and residual gas analyzer.

Mass flow controllers (MKS Instruments) are used to meter all gas feed rates. Reactants and diluent gas are introduced into the chamber via an injector that is packed with glass beads and a honeycombed screen. This imposes a well-defined plug-flow condition at the inlet. The injector head is 5.1 cm in diameter and can be translated vertically to position the inlet plane below the substrate. Typically, the distance between the stagnation plane and the inlet is 1.9 cm, which is less than the radius of the substrate, and therefore approximately 50% of the heated area will be correctly modeled by the one-dimensional stagnation-flow approximation under our experimental conditions (23). The active area of the substrate is 60% of the heated area, and therefore more than 80% of the active area is governed by ideal stagnation-flow behavior.

The substrate pedestal, which has the same diameter as the injector shower head, comprises a graphite heating element coated with boron nitride (Boralectric heater from Advanced Ceramics) mounted into a stainless steel block. The entire assembly is suspended by steel rods attached to the top of the reactor. A polycrystalline platinum foil 0.025 cm thick is fastened to the heating element with metal clips. Line voltage routed through a variable A/C transformer is used in an open loop to control heater power and therefore substrate temperature. A type-K thermocouple spot-welded to the Pt foil is used to record surface temperature. Additional thermocouples mounted within the injector measure gas temperature at the inlet centerline and radius of the shower head.

The reactor exhaust is throttled, allowing feedback control of the chamber pressure to any desired set point within the range 5–700 Torr. Residence times are determined by mass flow rate, reactor pressure, and temperature. Gases exiting the stagnation flow reactor are analyzed for chemical content using a mass spectrometer. The mass analyzer is housed within a separate chamber maintained at 5×10^{-9} Torr base pressure by a turbomolecular pump. Single-stage reduction from reactor to analyzer pressure is accomplished with a precision variable-leak valve. During sampling, pressure in the spectrometer chamber is increased to 1×10^{-6} Torr, which ensures that permanent vacuum gases contribute less than 0.5% to the recorded ion signals. Ions are created by electron impact and detected with an electron multiplier. A computer is used to log mass scans and thermocouple output at a rate of 0.1 Hz.

H_2 and O_2 were monitored by their respective parent-ion signals at mass/charge ratios (m/e) of 2 (H_2^+) and 32 (O_2^+). Due to potential interference from other species in the mixture, ion fragments at $m/e = 15$ (CH_3^+) and $m/e = 27$ ($C_2H_3^+$) were used to track CH_4 and C_2H_6. Product species

such as H_2O and CO were observed at $m/e = 18$ (H_2O^+) and 28 (CO^+). The carbon monoxide signal could not be resolved in mixtures of ethane, and therefore CO production rates are reported for methane only. The ion signal for CO_2 at $m/e = 44$ (CO_2^+) was not discernible above vacuum levels, and therefore this species was not considered a significant product of the reaction.

Mass flow controllers were used to calibrate the sampling system for O_2, CH_4, and C_2H_6 in mixtures of He and H_2. Production rates for H_2O were calculated using calibration factors measured from O_2 conversion in the absence of hydrocarbon. In the $H_2 : O_2 : CH_4$ experiments, the mole fraction of CO was calculated from the measured conversion of O_2, and the relative total ion currents for H_2O and CO were weighted by their respective total ion cross section (24, 25). Combined systematic and random errors in the determination of O_2 mole fractions are estimated to be $\pm 10\%$ at the 95% confidence interval; those for H_2O and CO are greater.

The reactions among H_2, O_2, and CH_4 or C_2H_6 over Pt were investigated at surface temperatures between 1000 and 1200 K at a reactor pressure of 10.0 ± 0.3 Torr. Reactants, supplied by Matheson, were of 99.99% initial purity and used without further purification. Helium was also used as a diluent to maintain a total constant flow rate during experiments where oxygen and hydrocarbons were incrementally added to the feed. Unless noted otherwise, the data presented here were collected under the following conditions: a total gas flow rate of 4500 $cm^3\ min^{-1}$, an $H_2 : O_2 : He$ mixing ratio of 4 : 1 : 3, and either CH_4 or C_2H_6 added incrementally in place of He up to 20 or 10% of the total flow, respectively.

A typical experimental run involved establishing a baseline reactor condition of 4 : 1 $H_2 : O_2$ in helium at constant power input, waiting for the surface temperature to stabilize, recording initial process variables, adding hydrocarbon to the feed, logging all system variables for 250 s, and then repeating the procedure for a new hydrocarbon mixture fraction. At the conclusion of the experiment, the reactor conditions were restored to the baseline and catalytic activity, in terms of water production and autothermal surface temperature, was evaluated with respect to the initial state. In addition, hydrocarbon mixture fractions were varied so that hysteretic effects on the surface reactivity could be evaluated.

Numerical Method

A one-dimensional stagnation flow model (Spin) was used to simulate experimental conditions in order to further investigate the heterogeneous production of water, as well as test the accuracy of a complex mechanism proposed for partial oxidation in short-contact-time reactors. The Spin program, developed at Sandia National Laboratories as part of the Chemkin collection of software tools (26), computes species, temperature, and velocity profiles in a steady-state, one-dimensional rotating disk or stagnation-point flow reactor. The program accounts for finite-rate gas-phase and surface chemical kinetics, in addition to multicomponent molecular transport. The governing differential equations form a 2-point boundary value problem that is solved by a modified Newton algorithm. The Spin program runs in conjunction with Chemkin, Surface Chemkin, and Transport utility software packages that facilitate the definition of gas-phase and surface chemical reaction mechanisms and thermodynamics, as well as managing transport properties. For a more detailed description of the numerical procedure, refer to (26).

The Spin code produces a one-dimensional solution to the stagnation flow problem. By similarity, the temperature and species concentrations in the flow field are independent of radius from inlet to substrate. The experiment measures species mole fractions of a well-mixed body of fluid near the exhaust of the reactor. To compare to the model, the one-dimensional Spin solution must be averaged to represent the bulk mixture. In this work, a treatment similar to that of Takeno and Nishioka (27) is used to calculate bulk mixture properties from a prediction of species concentrations along the axis perpendicular to the stagnation plane.

Following Takeno, the integral of the species equation within a cylindrical control volume results in the following expression at steady state:

$$\dot{s}_k W_k + \int_0^L \dot{\omega}_k W_k \, dx = (\rho u Y_k)_L + 2 \int_0^L \rho V Y_k \, dx. \qquad [1]$$

Definitions for notation can be found under Appendix: Nomenclature. The two terms on the left-hand side of Eq. [1] represent the mass production rates of species k at the surface and within the gas-phase control volume, respectively. To orient the reader, the inlet plane is at $x = L$, the surface or stagnation plane is at $x = 0$, and the direction of inlet flow velocity is negative from L to 0. Terms on the right-hand side of Eq. [1] represent mass inflow at $x = L$ and mass transported radially out of the control volume. Note that the term involving ρV is a function only of x (27). The average mole fraction for species k transported from the control volume is defined according to

$$X_k = \left(\frac{\int_0^L \rho V Y_k \, dx}{\int_0^L \rho V \, dx} \right) \cdot \left(\frac{\bar{W}}{W_k} \right), \qquad [2]$$

and is solved by integrating the discretized solution from Spin (ρ, V, and Y_k as functions of x) using the trapezoid rule. The total number of gridpoints in the solution field is refined automatically according to predetermined tolerance specifications to minimize numerical errors.

A detailed kinetic model, taken from a recent publication by Zerkle *et al.* (19) describing the oxidation of H_2,

CH_4, and C_2H_6 over platinum in an SCTR, was used as the model chemistry in the Spin calculations. The mechanism comprises 337 elementary reactions between 63 species and includes an extensive gas-phase hydrocarbon oxidation submodel and surface chemistry of both C_1 and C_2 hydrocarbon species.

In addition to the 255 gas-phase reactions, Zerkle *et al.* assembled from various literature sources a thermodynamically consistent surface mechanism composed of 82 reactions among 20 species. The elementary kinetics that compose the surface mechanism were extracted from reports describing observations made over pure platinum, and therefore can be used without modification. We anticipate that in our system the effect of support material on the kinetics are negligible. Thus far, the mechanism has been used to successfully predict the concentrations of C_2H_4 and other species exiting an SCTR catalytic monolith during partial oxidation of C_2H_6 in the presence of H_2. For more details regarding the kinetic model, the reader is referred to the original citation and references therein.

Regarding the investigation of heterogeneous water production in the $H_2 : O_2 : C_xH_{2x+2}$ system ($x = 1, 2$), the model chemistry was used in its entirety, with the exception of two modifications. The preexponential factors for reactions 57 and 59 in Zerkle *et al.* (19) were found to be in error and were corrected for this work; essentially the kinetic parameters were transposed in the journal publication. In addition, first-order sensitivity analysis revealed the importance of the O_2 sticking coefficient for the predicted result, and therefore it was allowed to vary from the number adopted by Zerkle *et al.* Values selected for the O_2 sticking coefficient are commensurate with the range of reported uncertainties on polycrystalline platinum foils (8, 28, 29).

Finally, to predict accurate values for Pt surface temperature after lighting off, a conduction term that accounted for heat loss from the backside of the substrate was introduced into the boundary condition of the energy equation. It was assumed that the conductive element was 1.3 cm thick and had the thermal properties of stainless steel (essentially the support material for the heater assembly). The power input to the heater, along with the gas temperature at the centerline of the inlet, was measured under every experimental condition and supplied as input to the model. To close the energy balance, the temperature at the backside of the substrate (T_{BACK}) used in the model was adjusted until good agreement was achieved between measured and predicted substrate temperatures. As defined, the conductive term represents a first-order approximation to heat-loss mechanisms in this system, with the exception of radiative processes which are adequately described in the governing equations. In all likelihood, the resultant T_{BACK} is not a true measure of the backside temperature; however, had this value been known, we would have then assumed a different thermal conductivity and/or thickness of conductive body at the boundary to arrive at the same result.

TABLE 1

Model Parameters Used in Spin Calculations

Parameter	Value	Units
Length of computational domain, (L)	1.91	cm
Pressure	0.0132	atm
Thermal conductivity of stainless steel	0.255	W cm^{-1} K^{-1}
Reactive site density for platinum surface	1.63×10^{15}	cm^{-2}
Pre-exponential factor for reaction R57[a]	7×10^{12}	s^{-1}
Pre-exponential factor for reaction R59[a]	1×10^{13}	s^{-1}
T_{LOW}:		
Inlet temperature boundary condition	564	K
Inlet velocity boundary condition	580	cm s^{-1}
Power input to substrate	1.4×10^8	erg cm^{-2} s^{-1}
T_{HIGH}:		
Inlet temperature boundary condition	696	K
Inlet velocity boundary condition	716	cm s^{-1}
Power input to substrate	3.1×10^8	erg cm^{-2} s^{-1}

[a] Corrected pre-exponential factors for reactions listed in Zerkle *et al.* (19).

Listed in Table 1 are various input parameters used in the Spin calculations, such as inlet boundary conditions, length of the computational domain, pressure, and values for the corrected pre-exponential factors. All experimental conditions were simulated in order to test the predictive capability of the model chemistry, as well as to elucidate the effects of hydrocarbon on the heterogeneous production of H_2O from rich mixtures of H_2 and O_2 over a Pt foil in stagnation flow.

3. RESULTS

Hydrogen/Oxygen System

Mixtures of $4:1:3$ $H_2 : O_2 : He$ served as baseline conditions for water production and autothermal activity to which all observations were referenced. At this mixing ratio, approximately 25 to 30% of the O_2 in the inlet was converted to H_2O, resulting in a net increase (ΔT) in the Pt surface temperature of 120 to 140 K. In this system the conversion of oxygen is limited by the combined effects of surface kinetics (low initial sticking probably for O_2) and reactant bypass. The small overall dimensions of the flow field coupled to the large inlet velocity within the stagnation geometry allow a high percentage of oxygen in the feed to blow by the heated substrate. Furthermore, there was little evidence to suggest that any homogenous chemistry occurred under these reactor conditions.

In order to verify this hypothesis, experiments were performed on mixtures approaching stoichiometry from the rich side to identify fuel-to-oxygen ratios that would support combustion. Ignition occurred at $H_2 : O_2$ mixing ratios of $4 : 1.75$, as evidenced by a bright region of incandescence in the center of the showerhead where presumably a flame was stabilized. The transition to homogeneous combustion

was abrupt, and in this instance the mass spectrometer indicated that all O_2 was consumed within the reactor. Results of Spin calculations further support the supposition that homogeneous chemistry is not important under our baseline conditions. Numerical predictions of species concentration changed by less than 0.5% at 1200 K when all gas-phase chemistry was omitted.

Figure 2 illustrates the steady-state surface temperature for 4 : 1 : 3 $H_2 : O_2 :$ He mixtures measured after lighting off as a function of surface temperature prior to lighting off. In the no-lighting-off case, H_2 and He were the only components in the feed, and the power input to the heater was fixed to achieve the reported temperature. The lighting-off condition was attained by replacing equal parts of He with O_2 on a molar basis up to 4 : 1 $H_2 : O_2$. The solid line in Fig. 2 is the substrate temperature predicted by Spin. Regardless of the initial surface temperature within the investigated range of conditions, only 25 to 30% of the O_2 was converted to H_2O, yielding a net energy flux to the surface that was nearly invariant with respect to the initial temperature. This, combined with the open-loop control on the substrate heater, produced the linear functionality displayed in Fig. 2.

Figure 3 presents the measured and predicted mole fractions for O_2, downstream from the stagnation plane, as a function of Pt surface temperature and initial O_2 sticking probability at 1000 and 1200 K. The solid and dashed lines in the figure are the results of Spin calculations at various values of the initial sticking probability for oxygen. The uppermost curve (solid line) is the value adopted by Zerkle *et al.* (19) and carries an inverse temperature dependence of the form $\gamma_o(O_2) = 0.07 \times (300/T(K))$. The experimental observations are bracketed above by the value reported by Zerkle *et al.* and below by $\gamma_o(O_2) = 0.09$. For this work, better agreement between model prediction and experiment, in terms of both the total amount of O_2 consumed and the subtle temperature dependence, is achieved by using a larger value for O_2 sticking probability. Thus, the simple $H_2 : O_2$ system performed essentially as predicted by the Zerkle *et al.* mechanism.

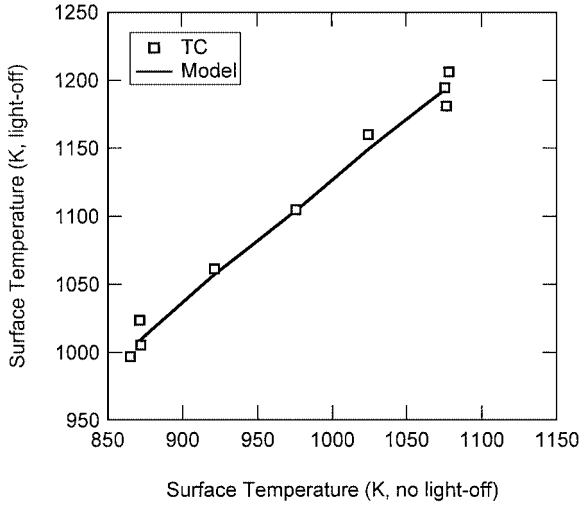

FIG. 2. Surface temperature of polycrystalline Pt foil at lighting off as a function of temperature prior to lighting-off for the baseline $H_2 : O_2 :$ He mixing ratio of 4 : 1 : 3 at 10 Torr. Open symbols are measurements; solid line is the Spin prediction.

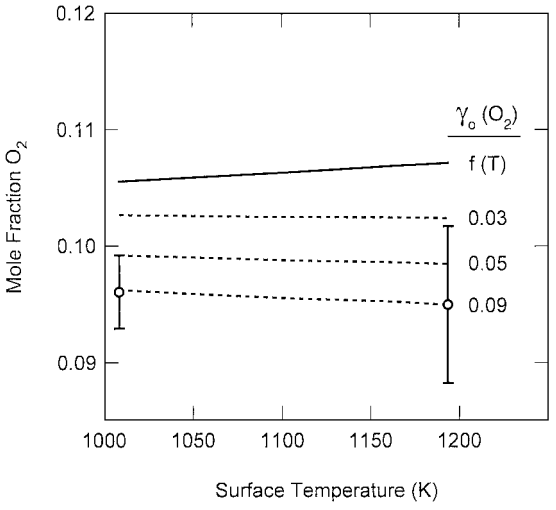

FIG. 3. Mole fraction of O_2 exiting the reaction zone as a function of surface temperature for the baseline condition. Open symbols are experimental data points; solid and dashed lines are Spin predictions at various initial sticking probabilities for O_2.

The fact that water-producing chemistry is relatively insensitive to substrate temperature and is completely heterogeneous under these hydrogen-rich conditions creates a unique platform with which to probe the effects of hydrocarbon on this system. Since the rate of O_2 consumption and subsequent heat release through hydrogen oxidation is nearly independent of the surface temperature, any deviation from baseline behavior may be attributed to the influence of added hydrocarbon as opposed to a change in temperature. Furthermore, the extent of gas-phase chemistry is negligible, and therefore surface-mediated processes are effectively isolated from those that occur in the gas phase. Here again, Spin calculations with and without full gas-phase chemistry indicate that hydrocarbons as well as H_2 and O_2 react primarily at the surface.

Hydrogen/Oxygen/Methane System

Helium was replaced by incremental amounts of CH_4 in the baseline mixture, up to 20%, in an effort to highlight any perturbation of the water-forming chemistry induced by the presence of hydrocarbon. Experiments were performed at five different temperatures in the range 1000 to 1200 K and at 12 different CH_4 mole fractions. Figures 4 and 5 illustrate the measured and predicted mole fractions for O_2, H_2O, and CO in the postreaction zone as a function of CH_4 concentration in the feed at 1000 K (T_{LOW}) and 1200 K (T_{HIGH}), respectively. Under the conditions of this

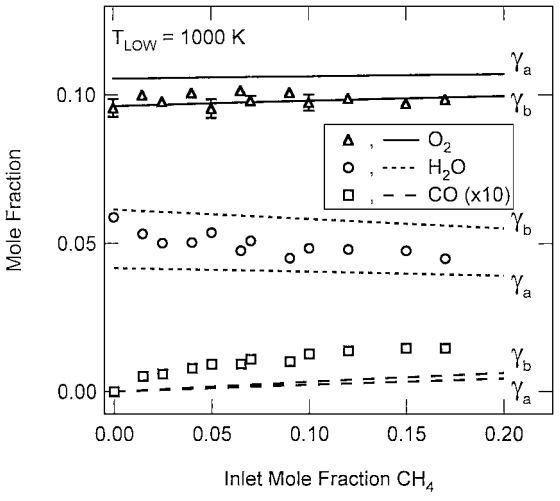

FIG. 4. Mole fractions of O_2, H_2O, and CO exiting the reaction zone as a function of the inlet mole fraction of CH_4 at 1000 K (T_{LOW}). Open symbols are experimental points; solid and dashed lines are Spin predictions at two different initial sticking probabilities for O_2 (γ_a = Zerkle *et al.* (19), $\gamma_b = 0.09$).

experiment, approximately 5 to 10% of the CH_4 was converted at 1200 K, and even less at lower temperatures. The solid and dashed curves in the figures are Spin predictions at two different initial O_2 sticking probabilities (γ_a = Zerkle *et al.*, $\gamma_b = 0.09$).

There are several noticeable trends in Figs. 4 and 5 that correlate with CH_4 concentration in the feed. First and foremost is that the concentration of H_2O decreases, dropping by 24% at T_{LOW} and by 36% at T_{HIGH} relative to baseline amounts (data points at CH_4 mole fraction 0.00), as the CH_4 content in the inlet increases. In addition, a small amount

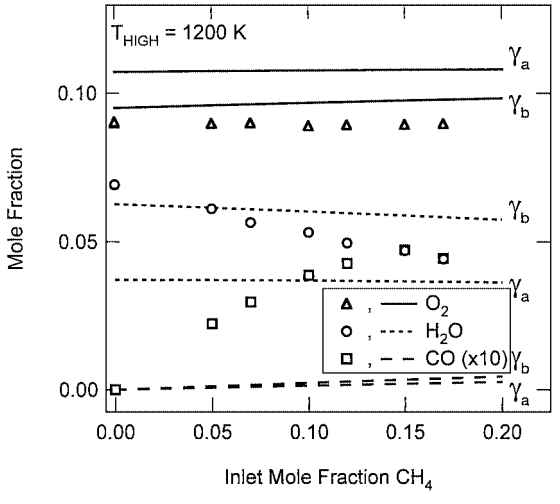

FIG. 5. Mole fractions of O_2, H_2O, and CO exiting the reaction zone as a function of the inlet mole fraction of CH_4 at 1200 K (T_{HIGH}). Open symbols are experimental points; solid and dashed lines are Spin predictions at two different initial sticking probabilities for O_2 (γ_a = Zerkle *et al.* (19), $\gamma_b = 0.09$).

of CO is produced, indicating that CH_4 is oxidized but not to any substantial degree. The absolute amount of CO appears to level off near 10% CH_4 in the inlet, which may indicate that beyond this mixture fraction O_2 becomes a limiting reactant in CO formation. Finally, the concentration of O_2 measured in the postreaction zone is not affected by the addition of CH_4 up to 20%, even though the H_2O concentration clearly decreases.

The results of Spin calculations are also presented in Figs. 4 and 5 and indicate that the model chemistry can predict the general trends observed in the experimental data, but fails to accurately capture the quantitative outcome. For instance, the simulations do indicate a downward trend in H_2O concentration with increased CH_4; however, the model chemistry predicts a moderate 6% decrease in H_2O concentration at T_{HIGH} as opposed to 36% observed experimentally. In addition, the mechanism proposed by Zerkle *et al.* (19) underpredicts the amount of CO formed, although a substantial error may be associated with the experimental measurement, because calibration factors for CO were inferred as opposed to being determined directly. The inconsistencies between model chemistry and experimental observation could not be adequately resolved by increasing the surface reactivity of O_2 (γ_b result versus γ_a), as was the case in the pure $H_2 : O_2$ system.

In addition to inhibiting water production, the presence of CH_4 in the reactor also has the effect of reducing the steady-state surface temperature at light-off. The temperature of the Pt foil is plotted in Fig. 6 as a function of inlet carbon fraction for T_{LOW} (lower graph) and T_{HIGH} (upper graph). Solid symbols represent data collected during the addition of CH_4 to the baseline mixture; the solid lines in this figure are linear least-squares fits. Since the formation of water is highly exothermic, a close coupling between surface temperature and rate of H_2O production is expected, given that the heater is under open-loop control at constant power. The data in Fig. 6 support this assertion; surface temperatures decrease with the decrease in H_2O production induced by the presence of CH_4 in the inlet.

Hydrogen/Oxygen/Ethane System

The effects of introducing C_2H_6 into the $H_2 : O_2$ baseline mixture were more pronounced than those for the CH_4 addition. As in the previous case, C_2H_6 was added incrementally in place of helium. However, the ethane content did not exceed 10% in order to maintain an equivalent carbon concentration between the two experiments on a per mole basis. Moreover, measuring the effect of C_2H_6 on the heterogeneous water-producing chemistry was more difficult than for that of CH_4 due to a steady decrease in the surface activity caused by carbon accumulation on the surface. While baseline reactivity of the Pt foil in terms of water production and light-off temperature could eventually be

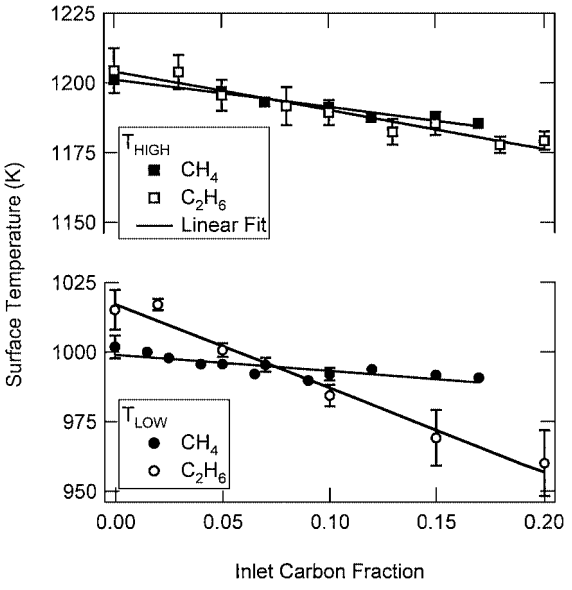

FIG. 6. Surface temperature of Pt foil as a function of the inlet carbon fraction, at 1200 K (T_{HIGH}, upper graph) and at 1000 K (T_{LOW}, lower graph), for addition of both CH_4 and C_2H_6 to baseline condition. Closed symbols are experimental data for CH_4; open symbols are experimental data for C_2H_6; solid lines are linear least-squares fits.

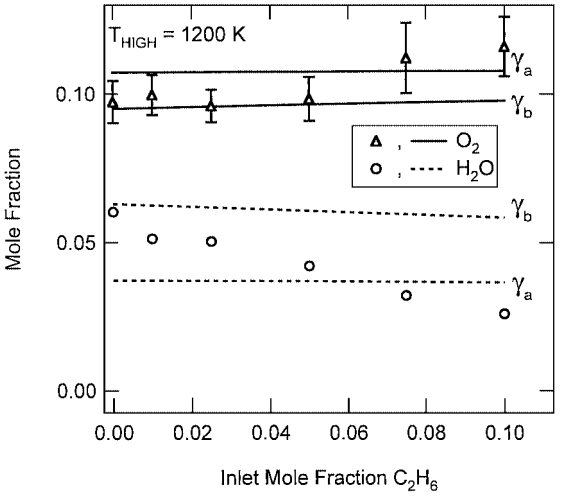

FIG. 8. Mole fractions of both O_2 and H_2O exiting the reaction zone as a function of the inlet mole fraction of C_2H_6 at 1200 K (T_{HIGH}). Open symbols are experimental points; solid and dashed lines are Spin predictions at two different initial sticking probabilities for O_2 (γ_a = Zerkle *et al.* (19), $\gamma_b = 0.09$).

recovered, the time required to achieve the initial state was longer than 250 s. This resulted in a pronounced hysteresis in the experimental data when the ethane mixture fraction was decreased from 10 back to 0%.

Figures 7 and 8 illustrate the measured and predicted mole fractions for O_2 and H_2O in the postreaction zone as a function of C_2H_6 concentration in the inlet at T_{LOW} and T_{HIGH}, respectively. Carbon monoxide was omitted because its spectral features could not be adequately resolved above those of C_2H_6 and of other possible C_2 hydrocarbon products at m/e 28. Under the conditions of this experiment, approximately 10 to 20% of the C_2H_6 was converted at 1200 K. The solid and dashed curves in the figures are Spin predictions at two different initial O_2 sticking probabilities (γ_a = Zerkle *et al.*, $\gamma_b = 0.09$).

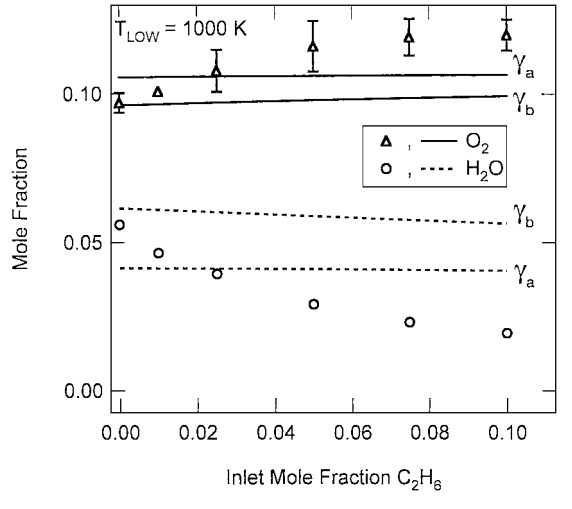

FIG. 7. Mole fractions of both O_2 and H_2O exiting the reaction zone as a function of the inlet mole fraction of C_2H_6 at 1000 K (T_{LOW}). Open symbols are experimental points; solid and dashed lines are Spin predictions at two different initial sticking probabilities for O_2 (γ_a = Zerkle *et al.* (19), $\gamma_b = 0.09$).

Two significant differences between the effects of C_2H_6 and those of CH_4 are evident in these figures. The first is that C_2H_6 exerts a greater influence on the water chemistry, causing a 60 to 65% decrease in H_2O concentration measured in the postreaction zone relative to that in the baseline condition. Second, the amount of O_2 consumed decreases along with the decreased water production, resulting in a larger concentration of O_2 in the reactor outlet as the amount of C_2H_6 in the feed increases. There also appears to be an abrupt transition in the O_2 concentration at 6% C_2H_6 for T_{HIGH}, as if the O_2 reactivity dropped significantly beyond a certain C_2H_6 concentration. Although the effect is difficult to discern in the T_{LOW} data, it is evident and more pronounced over the entire data set, which comprises five temperatures in the range 1000 to 1200 K. In addition, the transition point is temperature sensitive in that it moves toward higher ethane fractions at higher temperatures. The model chemistry fails to capture any of these significant differences between CH_4 and C_2H_6. Essentially, the results of Spin calculations shown in Figs. 7 and 8 are indistinguishable from those in the case of CH_4.

Finally, the lighting-off temperature of the Pt foil is also dependent on the amount of C_2H_6 in the reactor. Consulting the two graphs in Fig. 6, where the open symbols represent data collected during C_2H_6 addition, it is evident that

increasing the carbon fraction in the inlet causes the surface temperature to decrease. A greater effect is observed for C_2H_6 than for CH_4, indicating that the ethane surface chemistry is more efficient at inhibiting water formation. In fact, for T_{LOW} with C_2H_6, the surface temperature plunges by 50 K at the highest carbon fraction. Consequently, it takes longer to recover the baseline activity at T_{LOW} as well.

4. DISCUSSION AND CONCLUSIONS

The most pertinent finding of this investigation is that both CH_4 and C_2H_6 inhibit the heterogeneous production of H_2O over Pt under hydrogen-rich conditions. This is evidenced by (i) a decrease in the concentration of H_2O measured in the postreaction zone and (ii) a decrease in the light-off temperature for the Pt foil as the inlet carbon fraction increases. While a strong correlation exists between net water production, lighting-off temperature, and mole fraction of hydrocarbon in the inlet, the same is not true for the oxygen content in the system. Figure 9 illustrates the percentage conversion of O_2 for T_{LOW} (lower graph) and for T_{HIGH} (upper graph) as a function of inlet carbon for both CH_4 and C_2H_6 experiments. In the case of methane, the O_2 conversion is independent of carbon in the feed, even though water production has diminished. In the case of ethane, the system exhibits nonlinear behavior in the consumption of O_2 with conversion dropping by a factor of 2 or more at the highest carbon content investigated.

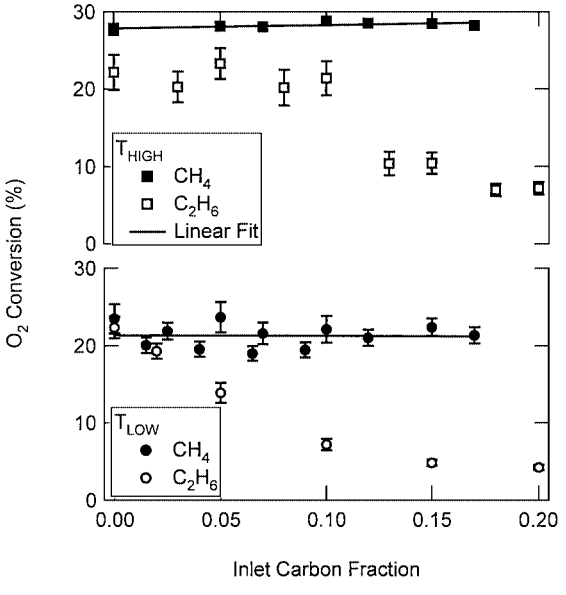

FIG. 9. Percentage conversion of O_2 in the stagnation flow reactor as a function of the inlet carbon fraction, at 1200 K (T_{HIGH}, upper graph) and at 1000 K (T_{LOW}, lower graph), for the addition of both CH_4 and C_2H_6 to baseline condition. Closed symbols are experimental data for CH_4; open symbols are experimental data for C_2H_6; solid lines are linear least-squares fits.

The exact nature of these effects is open to speculation. In the reducing environment of the stagnation flow experiments, both CH_4 and C_2H_6 could deposit carbon on the Pt foil, thereby blocking sites for O_2 and/or H_2 adsorption. This is certainly the case with C_2H_6 at 1000 K, where a visible carbonaceous film will grow within minutes of exposure. The simple fact that CH_4 has a lower sticking probability than C_2H_6 on Pt could explain the dramatic differences in the observed phenomena. The inhibition mechanism could also involve partially oxidized carbon species such as CO, even though conversion of hydrocarbon reactant is fairly low.

Alternatively, *homogenous* steam reforming of hydrocarbon may be responsible for generating CO and H_2 from the desorbed water, thereby decreasing the concentration of water measured in the exhaust but not inhibiting its formation at the surface. In order to investigate this possibility, simulations were performed using only the homogenous portion of the kinetic mechanism (surface chemistry switched off) proposed by Zerkle *et al.*, as well as GRI-Mech (30), on gas mixtures containing H_2, O_2, H_2O, and hydrocarbon at temperatures well above our experimental conditions. These calculations revealed that steam reforming becomes significant at temperatures in excess of 1500 K for the pressure and gas inlet velocities employed in this investigation.

While the mechanism by which hydrocarbon inhibits water formation on the platinum surface is unknown, these observations are highly relevant to the partial oxidation of ethane in SCTRs, because the feed compositions to these systems are rich in hydrocarbon and often contain hydrogen as well (19, 31). According to one interpretation of the basic operation of an SCTR, the exothermicity of water-forming chemistry provides the necessary heat to drive the endothermic dehydrogenation of C_2H_6. Both CH_4 and C_2H_6 can inhibit this process.

Finally, the model chemistry proposed by Zerkle *et al.* (19) cannot quantitatively reproduce the results of our stagnation flow experiments, nor can it qualitatively predict differences between the C_1 and C_2 effects. At this point the source of this discrepancy is unclear; however, the surface mechanism proposed by Zerkle *et al.* is deficient in pertinent carbon chemistry that was included in previous reports (17, 19).

The majority of the hydrocarbon reactions proposed by Zerkle *et al.* were taken from Wolf *et al.* (17), with the exception of several reactions involving ethylidyne and related C_2H_x species ($x = 1$–3). The largest differences between the Zerkle *et al.* chemistry and its primary source are the adsorption coefficients for both C_2H_6 and C_2H_4 and the omission of detailed C_2 chemistry leading to the formation of graphite. To achieve a better fit to experimental data in their SCTR simulations, Zerkle *et al.* adopted a sticking coefficient of 0.015 for both C_2H_6 and C_2H_4;

that reported by Wolf *et al.* for their work on oxygen-free methane conversion is unity. The difference is nearly two orders of magnitude. Unfortunately, increasing the ethane and ethylene sticking coefficients in the Zerkle *et al.* model is not sufficient to reproduce our experimental result using the Spin code. However, better agreement is obtained between predicted and observed hydrocarbon conversions. It is our belief that a combination of a near-unity sticking coefficient for C_2H_6 and the inclusion of C_2 chemistry leading to partial graphitization and therefore deactivation of the surface is needed to reconcile the model chemistry with the experiment.

5. APPENDIX: NOMENCLATURE

Symbol	Description	Units
$\dot{s}$	production rate of kth species due to surface reactions	mol cm^{-2} s^{-1}
u	axial velocity	cm s^{-1}
V	scaled radial velocity	s^{-1}
W_k	molecular weight of kth species	g mol^{-1}
$\bar{W}$	mean molecular weight of mixture	g mol^{-1}
x	axial coordinate	cm
X_k	molar fraction of kth species	
Y_k	mass fraction of kth species	
$\dot{\omega}_k$	production rate of kth species due to gas-phase reactions	mol cm^{-3} s^{-1}
ρ	mass density	g cm^{-3}

ACKNOWLEDGMENT

This work was supported by the U.S. Department of Energy, Office of Industrial Technologies Chemical Industry of the Future Team.

REFERENCES

1. Hickman, D. A., and Schmidt, L. D., *AICHE J.* **39**, 1164 (1993).
2. Bodke, A. S., Bharadwaj, S. S., and Schmidt, L. D., *J. Catal.* **179**, 138 (1998).
3. Huff, M., and Schmidt, L. D., *J. Phys. Chem.* **97**, 11,815 (1993).
4. Koltsakis, G. C., and Stamatelos, A. M., *Prog. Energy Combust. Sci.* **23**, 1 (1997).
5. Shelef, M., and McCabe, R. W., *Catal. Today* **62**, 35 (2000).
6. DallaBetta, R. A., *Catal. Today* **35**, 129 (1997).
7. Burch, R., Crittle, D. J., and Hayes, M. J., *Catal. Today* **47**, 229 (1999).
8. Ljungstrom, S., Kasemo, B., Rosen, A., Wahnstrom, T., and Fridell, E., *Surf. Sci.* **216**, 63 (1989).
9. Hellsing, B., Kasemo, B., and Zhdanov, V. P., *J. Catal.* **132**, 210 (1991).
10. Williams, W. R., Marks, C. M., and Schmidt, L. D., *J. Phys. Chem.* **96**, 5922 (1992).
11. Warnatz, J., Allendorf, M. D., Kee, R. J., and Coltrin, M. E., *Combust. Flame* **96**, 393 (1994).
12. Rinnemo, M., Deutschmann, O., Behrendt, F., and Kasemo, B., *Combust. Flame* **111**, 312 (1997).
13. Deutschmann, O., Behrendt, F., and Warnatz, J., *Catal. Today* **46**, 155 (1998).
14. Deutschmann, O., and Schmidt, L. D., *AICHE J.* **44**, 2465 (1998).
15. Schmidt, L. D., Deutschmann, O., and Goralski, C. T., *Stud. Surf. Sci. Catal.* **119**, 685 (1998).
16. Wolf, M., Deutschmann, O., Behrendt, F., and Warnatz, J., *Stud. Surf. Sci. Catal.* **119**, 271 (1998).
17. Wolf, M., Deutschmann, O., Behrendt, F., and Warnatz, J., *Catal. Lett.* **61**, 15 (1999).
18. Deutschmann, O., Maier, L. I., Riedel, U., Stroemman, A. H., and Dibble, R. W., *Catal. Today* **59**, 141 (2000).
19. Zerkle, D. K., Allendorf, M. D., Wolf, M., and Deutschmann, O., *J. Catal.* **196**, 18 (2000).
20. Burch, R., Urbano, F. J., and Loader, P. K., *Appl. Catal. A* **123**, 173 (1995).
21. Ciuparu, D., and Pfefferle, L., *Appl. Catal. A* **209**, 415 (2001).
22. Marecot, P., Fakche, A., Kellali, B., Mabilon, G., Prigent, M., and Barbier, J., *Appl. Catal. B* **3**, 283 (1994).
23. Houtman, C., Graves, D. B., and Jensen, K. F., *J. Electrochem. Soc.* **133**, 961 (1986).
24. Rapp, D., and Englander-Golden, P., *J. Chem. Phys.* **43**, 1464 (1965).
25. Hwang, W., Kim, Y. K., and Rudd, M. E., *J. Chem. Phys.* **104**, 2956 (1996).
26. Kee, R. J., Rupley, F. M., Miller, J. A., Coltrin, M. E., Grcar, J. F., Meeks, E., Moffat, H. K., Lutz, A. E., Dixon-Lewis, G., Smooke, M. D., Warnatz, J., Evans, G. H., Larson, R. S., Mitchell, R. E., Petzold, L. R., Reynolds, W. C., Caracotsios, M., Stewart, W. E., Glarborg, P., Wang, C., and Adigun, O., CHEMKIN COLLECTION, Release 3.6, Reaction, Design, Inc., San Diego, CA, 2000.
27. Takeno, T., and Nishioka, M., *Combust. Flame* **92**, 465 (1993).
28. Hellsing, B., Kasemo, B., Ljungstrom, S., Rosen, A., and Wahnstrom, T., *Surf. Sci.* **189**, 851 (1987).
29. Pacia, N., Weber, B., and Pentenero, A., *Surf. Sci.* **49**, 330 (1975).
30. Smith, G. P., Golden, D. M., Frenklach, M., Moriarty, N. W., Eiteneer, B., Goldenberg, M., Bowman, C. T., Hanson, R. K., Song, S., Gardiner, W. C., Jr., Lissianski, V. V., Qin, Z., GRI-Mech 3.0, *available at* http://www.me.berkeley.edu/gri_mech/, 1999.
31. Bodke, A. S., Henning, D., Schmidt, L. D., Bharadwaj, S. S., Maj, J. J., and Siddall, J., *J. Catal.* **191**, 62 (2000).